The Astronomical Journal, 150:101 (13pp), 2015 October doi:10.1088/0004-6256/150/4/101

THE FIRST U.S. NAVAL OBSERVATORY ROBOTIC ASTROMETRIC TELESCOPE CATALOG

N. Zacharias[1], C. Finch[1], J. Subasavage[2], G. Bredthauer[3], C. Crockett[2], M. Divittorio[2], E. Ferguson[1], F. Harris[2], H. Harris[2], A. Henden[4], C. Kilian[1], J. Munn[2], T. Rafferty[5], A. Rhodes[2], M. Schultheiss[2], T. Tilleman[2], and G. Wieder[1]
[1] U.S. Naval Observatory, Washington, DC 20392, USA; nz@usno.navy.mil
[2] U.S. Naval Observatory Flagstaff Station, AZ 86001, USA
[3] Semiconductor Technology Associates, San Juan Capistrano, CA 92675, USA
[4] AAVSO, 49 Bay State Rd., Cambridge, MA 02138, USA
Received 2015 March 28; accepted 2015 July 27; published 2015 September 3

ABSTRACT

URAT1 is an observational, astrometric catalog covering most of the $\delta \geqslant -15°$ area and a magnitude range of about $R = 3$–18.5. Accurate positions (typically 10–30 mas standard error) are given for over 228 million objects at a mean epoch around 2013.5. For the over 188 million objects matched with the Two Micron All Sky Survey (2MASS) point-source catalog proper motions (typically 5–7 mas yr^{-1} standard errors) are provided. These data are supplemented by 2MASS and AAVSO Photometric All-Sky Survey (APASS) photometry. Observations, reductions, and catalog construction are described, together with results from external data verifications. The catalog data are served by CDS, Starsbourg (I/329).

Key words: astrometry – catalogs – proper motions

1. INTRODUCTION

The U.S. Naval Observatory (USNO) Robotic Astrometric Telescope (URAT) project was conceived as the next step beyond the successful USNO CCD Astrograph Catalog (UCAC) project (Zacharias et al. 2013), providing accurate reference star positions on the sky at current epochs before *Gaia*[6] data become available. Original plans called for a new, dedicated 1 m class telescope (Zacharias 2002, 2004; Laux & Zacharias 2005; Zacharias et al. 2006). Primarily owing to its cost, the instrument was not built. However, the detector development initiated by a Small Business Innovation Research through the Office of Naval Research led to the manufacturing of the world's largest, monolithic detector, the STA1600. In 2008 funding became available for a large focal-plane instrument consisting of four of those 111 million pixel detectors. The USNO "redlens" astrograph Vukobratovich et al. (1992) previously used for the UCAC survey (Zacharias et al. 2013) was completely rebuilt by the USNO instrument shop in Washington, DC. A single truss-tube structure now joins the old lens and the new focal plane dewar, utilizing the 9 degree diameter field of view.

After initial tests in 2011 September in Washington, DC, the telescope was deployed to the Naval Observatory Flagstaff Station (NOFS) in Arizona in 2011 October. Upgrades to the dome for lightning protection were installed, subsequent hardware issues resolved, and operational robustness improved. Survey operations began in 2012 April.

A wide dynamic range of stars between about $R = 3$ and 18.5 mag are being observed with a combination of long exposures and short exposures with an objective grating. With multiple sky overlaps per year and its high precision, URAT is aiming at two specific goals: first, to establish a highly accurate, dense, deep optical reference frame at current epochs; and second, to identify nearby stars without selection effects by directly observing trigonometric parallaxes in an all-sky survey.

Unfortunately, the project was delayed owing to various technical and funding issues and is now running close to *Gaia* data releases. However, accurate reference stars in the northern hemisphere (URAT1) are available since 2015 March, over a year prior to an anticipated first *Gaia* data release. Northern hemisphere observing was completed in 2015 June, and the instrument is in transit for deployment to the southern hemisphere. More information about this project and potentially upcoming data releases is available at our Web page www.usno.navy.mil/USNO/astrometry/optical-IR-prod/urat.

The main purpose of URAT1 is to provide the astronomical community with a reference star catalog for current epochs about 4 times more precise than UCAC with a density similar to the Two Micron All Sky Survey (2MASS; Skrutskie et al. 2006), which is on average a factor of 4 improvement over UCAC4. Science drivers for accurate positions include assisting in predictions of solar system bodies' occultations, improving accuracy of positions of moving objects referenced to the sky background (inertial reference star catalog), and linking of the radio and optical coordinate systems.

Although URAT1 proper motions are very useful for stars fainter than the UCAC limit, they are only preliminary. Particularly for stars in the 8–14 mag range UCAC4 has better proper motions than URAT1, with correspondingly more precise positions at much earlier epochs than 2014.

URAT1 is neither complete (maybe on the 90% level) nor free of contamination (expected to be less than 0.5%). Systematic errors in positions are estimated to be on the 10 mas level, while systematic errors in proper motions are on the 1–2 mas yr^{-1} level.

The URAT1 catalog is presented as a collection of binary data files (total about 18 GB) with index file, auxiliary software, and info. These data are served by CDS, Strasbourg. There is no data release on DVD. This paper accompanies the URAT1 catalog release and provides the scientific rationale, reduction details, and results. Users of URAT1 are also referred to the "readme" file included with the data release.

[5] USNO, retired
[6] http://sci.esa.int/gaia, www.cosmos.esa.int/web/gaia

Table 1
Basic Data of the Telescope, Camera, and Survey Exposures Used for URAT1

Telescope	Astrograph	Value	Unit
	Aperture	203	mm
	Focal length	2060	mm
	Bandpass	680–762	nm
Camera	4 CCDs, each	10.5k × 10.5k	px
	Pixel size	9.0	μm
	Scale	0.905	”/px
	Size, each	95 × 95	mm
	Field of view	28	sq. deg
Guiding	3 CCDs, each	2k × 4k	pixels
	Scale	0.80	”/px
Regular	2 expos./field	60 and 240	s
Grating	2 expos./field	10 and 30	s

2. OBSERVATIONS

2.1. Instrument

Basic information about the telescope and camera is provided in Table 1. All observations utilize the same five-element “redlens” that was used for the UCAC program. A single, fixed bandpass (680–762 nm) is provided by the dewar window, which serves as a filter. The bandpass for URAT was pushed as far red as possible to reduce effects of atmospheric turbulence on the astrometry.

Focusing is performed by moving the lens because the backend dewar is much heavier than the lens. The dewar hold time is just over 24 hr, during which time about 25 kg of LN_2 are boiled off. To compensate for this change in weight, a counterweight is moved along an arm on the opposite side of the pier to keep the telescope balanced.

A custom-made shutter from Bonn University (Klaus Reif) is used. The layout of the focal plane is shown in Figure 1. The gap between the main CCDs (labeled A to D) is 1200 arcsec. Each of the four main CCDs covers a sky area of $2\overset{\circ}{.}65$ by $2\overset{\circ}{.}65 = 7$ square degrees.

For part of the observing program (see below) a diffraction grating is mounted in front of the lens. First-order diffraction images saturate for stars about 5.0 mag brighter than for the central images, thus expanding the dynamic range of the survey enormously. The STA1600 CCDs also feature clocked anti-blooming (CAB), which drains electrons near saturation to avoid bleeding of charge into neighboring pixels. This allows us to obtain accurate centroid fits of stars about 1.5–2.5 mag brighter than traditional saturation, thus further extending the dynamic range of URAT data toward bright stars. Figure 2 shows the brightness range of stars covered by various exposure times and modes of operation.

The STA1600 CCDs are backside illuminated with optimized quantum efficiency near the URAT bandpass. The CCDs have few to none column defects. The CCDs are operated normally at −100°C. Each main CCD has eight readout ports going to one side of the CCD. All four CCDs are read in parallel in about 20 s with a read noise of about 10 e^- rms. Full well capacity is at about 80 ke^-, and the gain is set to fully utilize the available dynamic range with 16 bit output.

A fiberglass dome with added metal mesh and other lightning protection measures is used. To improve the dome seeing, air is sucked out from the floor near the telescope mount, which provides a steady air flow down through the dome slit while observing.

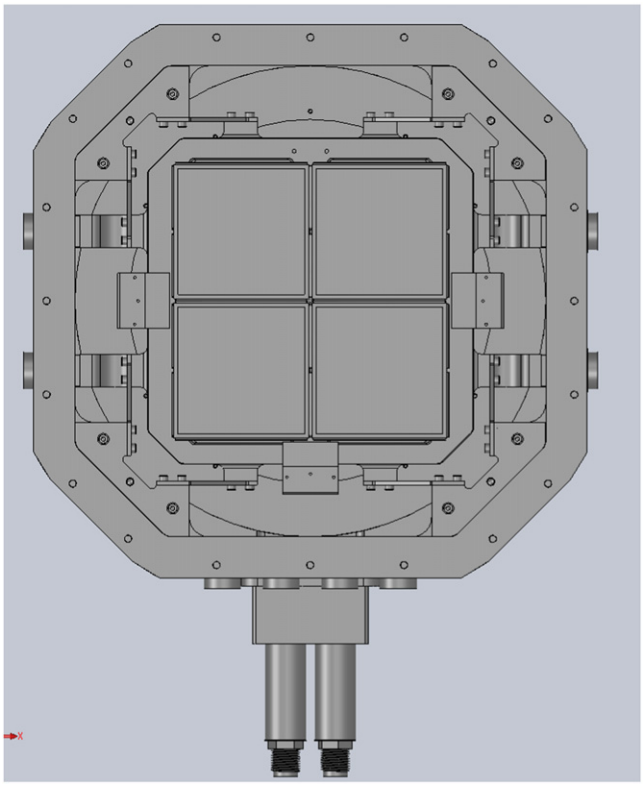

Figure 1. Layout of URAT focal plane. Each of the four big CCDs is 95 mm by 95 mm in size. There are three more CCDs (right, left, bottom) for guiding and focus determination.

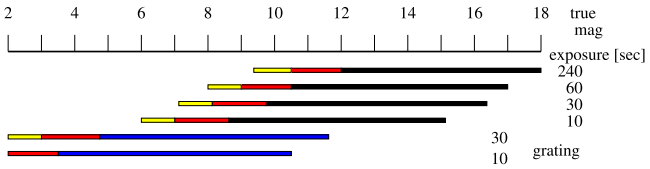

Figure 2. Dynamic range of various exposure times and modes of URAT data. Different shades in color represent from right to left: unsaturated regime (black and blue), saturated with CAB allowing good astrometric results (red), and saturated regime with lower-quality astrometric calibration (yellow).

2.2. Survey Fields and Exposures

A basic pattern of survey fields was adopted with the same gap size between adjacent telescope pointings CCD footprints as the gap size between the four CCDs in the focal plane. To fill in the gaps, two more of the basic patterns of fields were overlaid with diagonal offsets. For each of these three-times basic patterns of fields, a 5-fold dither pattern was adopted leading to a total of 15-fold overlap of fields. Owing to the gaps, this results in an average of 12 fields covering every area on the sky.

A 60 s and a 240 s exposure are taken on each such survey field. To cover a wide parallax factor range, the night is split into five parts of equal duration. Utilizing one dither position per part of the night, the corresponding three-times basic pattern of fields is observed during each part of the night. Thus, the entire pattern of 15 overlaps of fields is observed once per year. Priority is given to high-declination fields. The southern

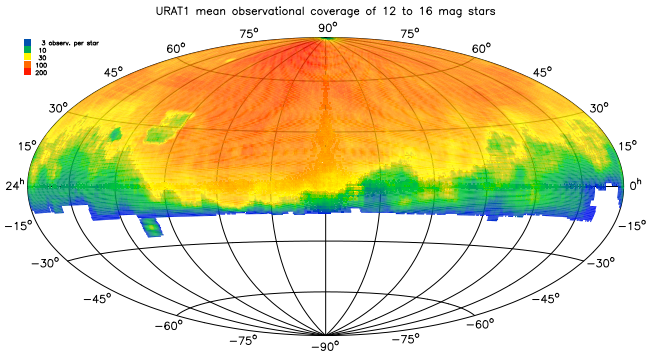

Figure 3. Sky coverage of URAT1 catalog data. Color coding indicates the average number of observations per star for stars between magnitude 12 and 16.

limit of the survey is then determined by the available hours of observing, which vary by season.

The above-mentioned regular survey operation is run for about three weeks in a month without an objective grating. During the week around full Moon, the same pattern is observed again with short exposures (mostly 10 and 30 s, sometimes 20 and 30 s) and with an objective grating mounted in front of the lens.

Figure 3 shows the mean number of observations per star (around magnitude 14, i.e., best case with data from almost any exposure) as found in the URAT1 catalog. More color plots, like the mean number of URAT1 stars per square degree, are provided with the data release in the "info" folder. URAT1 covers almost the entire northern sky and most of the area $\delta \geqslant -15°$, plus the far south area around Pluto.

2.3. Robotic Operations

The entire operation is controlled by a single Linux computer. The top-level URAT operations control software and reduction code are written in Fortran. C-code routines are called for hardware interfaces to three systems: telescope, main CCDs, guide CCDs. Most telescope functions are routed through a Galil controller. HomeDome provided an interface to control dome shutter and dome rotation.

Every afternoon an "observer" needs to come to the telescope to unhook the LN_2 line, verify safety of operations, and check on system status. A single command initiates auto-mode operations. The observer then notes the time of the LN_2 fill and paths to save/backup the night's data. The counter-weight position is then automatically calculated and moves to position. The system is then in a loop mode checking weather conditions and time. The dome automatically opens around sunset, and blowers turn on to equalize the temperature in the dome. A focus sequence is run and evaluated during twilight, and survey observations begin when skies are sufficiently dark. System e-mails are sent for dome open/close and emergency notifications. Observing progress can be monitored remotely with a command line interface.

The control software has a wait loop before each observation where weather and safety conditions are monitored. A Boltwood cloud sensor unit is used for checking weather conditions, and UPS units are monitored for power outages. In case of bad weather, the software will close the dome and wait for the conditions to improve. In case of power failure, UPS batteries are sufficient for the software to close the dome and power off the computers. A watch script is used to monitor the control code. If the software hangs up, the watch script will initiate a shutdown sequence, closing the dome and parking the telescope. The HomeDome system itself will shut down the dome if it loses communication with the control computer.

A triple fail-safe system is used to prevent the telescope from hitting something. Software limits are set for safe operations. In case they fail, optical limit switches stop the telescope motion. In case of a complete telescope control failure, Mercury limit switches directly cut power to the telescope motion in case it exceeds limits in telescope pointing with respect to the horizon.

At the end of the night the pixel data and log files are transferred via ftp to a second Linux computer and reductions and backups are initiated automatically, which sometimes run into early the next night. The "observer" or instrument shop personnel connects the LN_2 line sometime in the morning before the auto-fill begins. The only other human interaction is for putting the grating on/off once a month, checking on desiccant cartridges at the lens, changing hard disk drives about once every week or two, and troubleshooting. The project encountered a fair amount of down time early on owing to dome upgrades for lightning protection and associated side effects. Recent operations are very stable, with only occasional need for a reboot of the control computer and/or Galil interface and implementing control software fixes after mandatory operating system kernel updates.

2.4. Guiding and Focus Control

All exposures of 30 s duration or longer are guided. The three smaller CCDs mounted at the edge of the field of view are used to take about 4 s long exposures. These images are read out and evaluated in real time. Mean telescope pointing corrections are thus derived about every 6 s and fed to the mount before the next cycle of guide exposures begins.

The three guide CCDs are mounted at different distances with respect to the focal plane: intra-focal, in focus, and extra-focal. At the end of a guided exposure the mean observed image profile width of each guide CCD is used to adjust the focus if needed. The complex lens is sensitive to temperature and temperature history, so frequent (about 20) focus changes are performed throughout the night.

2.5. Quality Control

After the automatic pixel processing is completed, a project scientist generates and looks at five pages of quality control plots of the data of the previous night. Occasionally manual reductions are run in steps in case of a failure of a system. Flags indicating possible problems are raised automatically, and the project scientist has access to various, detailed log files for troubleshooting if needed.

Limits are set on mean image elongation, image profile width, saturation, and limiting magnitude for an exposure to meet survey quality. The mean numbers of detected objects per readout tab are compared to identify potential missing data. Rejected exposures are noted and picked up automatically by the scheduling software for next-night observations. The quality control pipeline was not fully available until the end of 2012, and early survey data were only spot-checked, with a few fields reobserved.

2.6. Darks, Flats, Photometry

Darks for all standard exposure times are taken several times per year. A few sets of sky flats were obtained throughout the project, taken near sunset with a piece of white cloth covering the lens. The pixel-to-pixel sensitivity variations are found to be small and stable. Emphasis of this program is on astrometry, and only minimal effort was put into providing URAT bandpass photometry. Survey quality observations often were obtained during partly cloudy nights or with cirrus present. No dedicated observations of photometric standard stars were performed, and all observations are taken within about 5° (20 minutes) of the meridian.

2.7. Astrometric Calibration Observations

For normal operations the astrograph is on the east side of the pier. A few times throughout the project, the telescope is flipped to the west side of the pier, allowing observations with the focal plane rotated by 180° with respect to the sky. The same field is observed on the same CCD in both orientations, allowing us to detect and calibrate possible magnitude-dependent systematic errors of star positions caused by the instrument alone. In another calibration observing run the same fields are being observed with the objective grating on and using short (typically 30 s) and long (240 s) exposures. Mapping of x, y centroid positions of stars observed with such pairs of exposures allows us to compare positions of the same stars as observed with first-order grating images and central images, as well as comparing data of saturated and non-saturated images of the same stars.

2.8. Data Used for URAT1

For the URAT1 catalog reduction 57,129 exposures (of a total of 65,639) from 2012 April 24 until 2014 June 21 were selected, meeting acceptable quality standards. A total of 14 and 12 exposures of the Pluto field area taken on 2013 September 19 and 2014 September 06, respectively, were added. These fields were observed to support occultation predictions. Altogether, data from 380 nights were used for URAT1. This includes some special observing like bright stars and astrometric calibration exposures (see above). The distribution of observations by month is shown in Figure 4. Clearly, a seasonal pattern is seen, with fewer exposures than average taken in winter and summer (monsoon). Grating survey observing became routine about half a year into the program.

A small fraction of data were dropped during the reduction process. In particular, if too few reference stars were matched or conventional astrometric solutions were poor, those exposures were just not included in upstream processing. Similarly, all individual "problem stars" like blended images were dropped.

The URAT data for this first release were split into 38 sets, 19 each for grating and regular survey data. All grating observations taken within about a week around each full Moon were collected into a set. All data taken between two such grating observing runs comprise a set of regular survey data. In a few cases with sparse data, a set extends over about seven weeks.

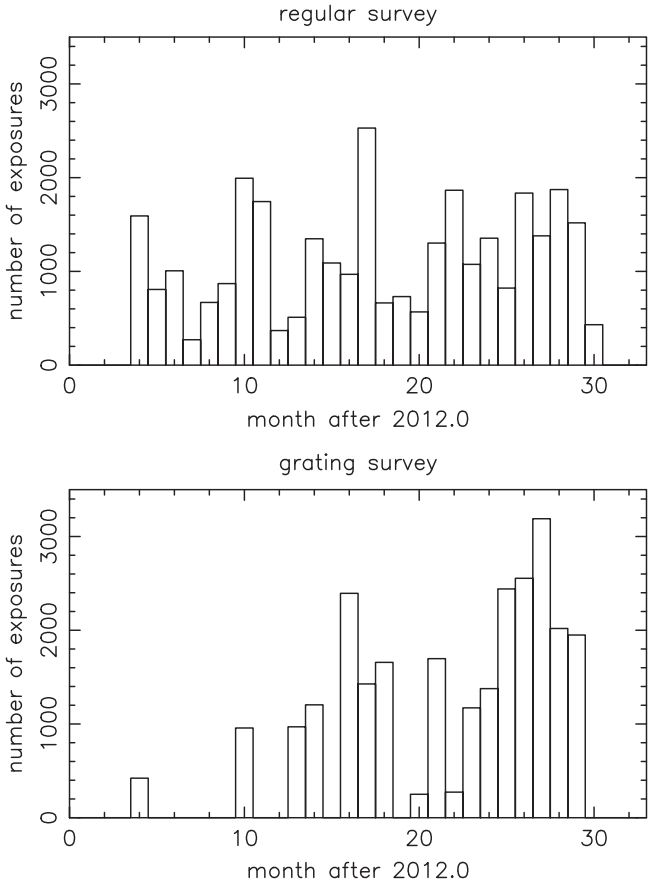

Figure 4. Number of exposures used for URAT1 by month after 2012.0 (4 is 2012 April, 13 is 2013 January). Data for the regular and grating survey are shown separately.

3. REDUCTIONS

The camera output is written to 2-byte unsigned integers in FITS format with very basic header data, while observing log files are kept as separate text files. All raw image processing, photometric, and astrometric reductions were performed with a custom Fortran code, building on the software used for the UCAC program. IRAF and DS9 were used to display sample data and perform image examinations for spot checks, algorithm development, and trouble shooting. Each of the four main camera CCDs was handled separately throughout the reductions, as if data were taken with a different telescope for each CCD.

3.1. Pixel Data and Centroids

Raw CCD exposures were bias corrected from overscan data. A mean dark of corresponding exposure time and epoch was subtracted and a mean flat applied. No extra bias frames were utilized.

Background level and noise were calculated from histogram data of subareas. Objects were detected with a threshold of 4σ above the background. Basic image profile properties like elongation and start parameters for the center fit were obtained from moment analysis of the pixels forming that image. Object centers were determined from a least-squares fit of the pixel data using a two-dimensional circular symmetric Gaussian image profile model function. Only objects with a successful fit were propagated to the next step in the reduction process.

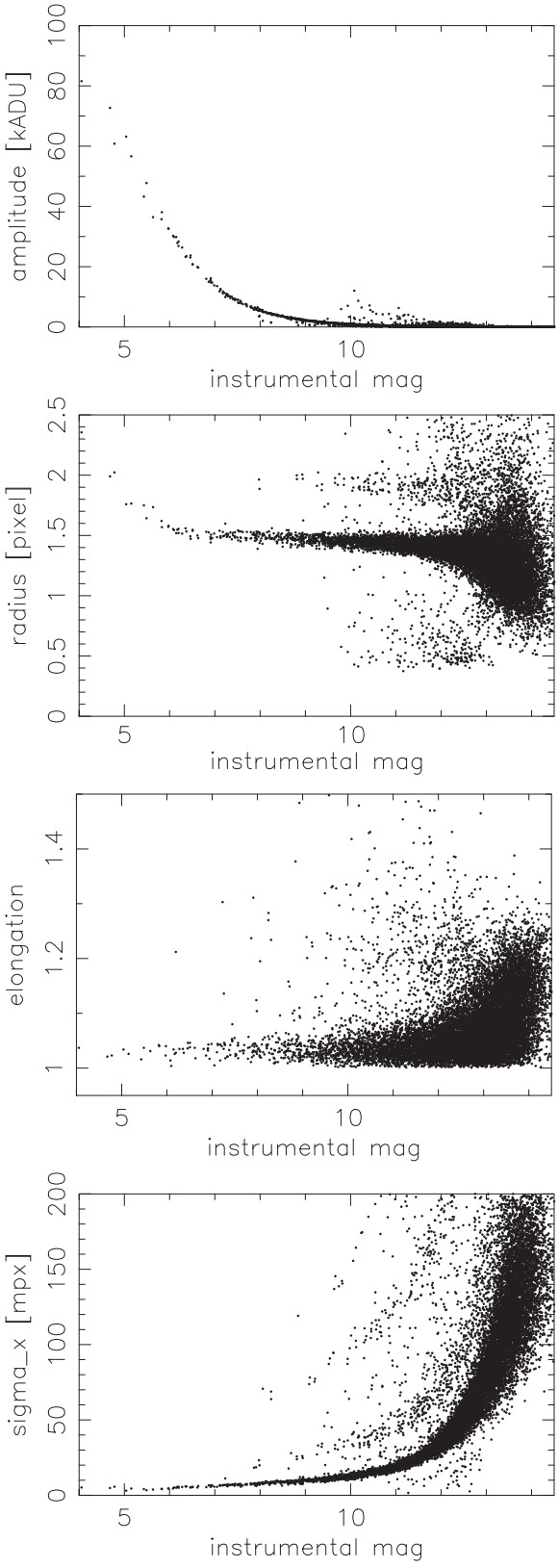

Figure 5. Individual stellar image profile fit results as a function of instrumental magnitude; from top to bottom: amplitude, radius, elongation, and center error per coordinate. Results for exposure 14064 (10 s) of CCD B are shown.

Figure 5 shows sample results for an exposure taken with the grating. The CAB feature of the CCD enables a dynamic range of almost 10 mag. Saturation is at about 30 kADU or instrumental magnitude 6.5. First-order diffraction images have an average elongation of about 1.1 (ratio of major to minor axis of image) and a significantly larger fit radius than the central images. The image center fit precision is below 10 millipixels over several magnitudes, including the CAB regime up to 2.5 mag brighter than the traditional saturation limit.

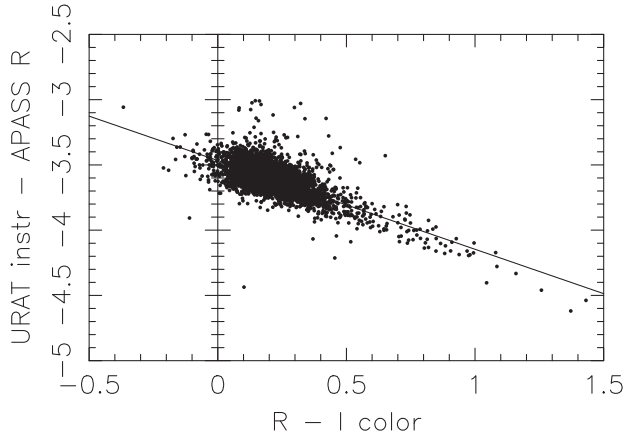

Figure 6. Example of color–color data correlation used to determine the photometric constant between URAT instrumental and calibrated magnitudes per exposure and CCD using APASS *R* and *I* data.

3.2. Photometry

Instrumental magnitudes were derived from the volume of the two-dimensional Gaussian image profile fits, not from aperture photometry. These magnitudes were calibrated with AAVSO Photometric All-Sky Survey (APASS) *R* and *R–I* data in a linear fit to derive a zero-point constant between the instrumental and calibrated URAT bandpass magnitudes. An example is given in Figure 6 for a single exposure and CCD. The formal error of a zero-point constant is typically around 0.01 mag. Many URAT observations were performed in nonphotometric conditions, and URAT photometry is believed to be accurate on a few percent level at best. Errors on URAT1 magnitudes as given in the catalog are derived from scatter of individual observations with 0.01 mag error floor rms added.

3.3. Grating Image Merge

For all grating exposures, individual images in the *x*, *y* data files were identified as belonging to a central or first-order or higher-order diffraction image by taking into account the brightness, location, and elongation information. The algorithm to identify these images was refined by looking at pixel data with the IRAF "tvmark" feature to highlight various types of images. An arithmetic mean position was calculated from a matching pair of first-order grating images. In addition, all central images were kept as separate observations. Thus, some stars have two observations per exposure based on central image and first-order diffraction images, respectively. All single first-order images and all higher-order images are rejected.

3.4. Astrometric Solution

A subset of the UCAC4 (Zacharias et al. 2013) stars, those with astrometry flag "good" and in the magnitude range of

8.0–16.0, were used as reference stars in a conventional, weighted least-squares adjustment of URAT data to obtain α, δ positions. Using our custom software, reference stars were matched with the x, y data utilizing telescope pointing data from the observing log files.

Owing to the large field of view, an eight-parameter plate model was adopted, which includes two tilt terms (p, q) besides the full linear model (a to f, split into orthogonal and nonorthogonal terms):

$$\xi = ax + by + c + ex + fy + px^2 + qxy$$

$$\eta = -bx + ay + d + fx - ey + qy^2 + pxy.$$

Here ξ, η are the standard coordinates (scaled from radian to arcsec) and x, y the observed center coordinates of star images on the CCD (scaled from pixel unit to arcsec). This approach is feasible owing to the large number of reference stars available per CCD, ranging from a few hundred to several thousand.

The root-sum-square formal errors of UCAC4 reference star positions at URAT observing epochs, the formal errors of URAT x, y data, and an atmospheric turbulence contribution (20 mas for 100 s exposure, scaled by square root of exposure time) were used as weights in the astrometric solution. For most stars the largest error contribution is from the UCAC4 proper motion errors. Fit results after excluding over 3σ outliers show on average only about 10% larger values than expected from the combination of all known, estimated error contributions, which easily could have been underestimated by that amount.

Astrometric solution errors are independent of the number of reference stars available for individual exposures. There is a significant variation of the astrometric solution error as a function of declination, which can be explained by the mean epoch differences between URAT1 and UCAC4 data. The area near the celestial north pole was observed last in the UCAC4 program, leading to the smallest epoch differences to URAT1 data and thus to the smallest UCAC4 position errors at URAT1 epoch due to error propagation of the UCAC4 proper motion errors.

The CCDs were found to be aligned to α, δ to within $13'$ and $36'$, with x being along δ. The plate tilt parameters were found to be significant and vary as expected by zenith distance (telescope tube bending and other effects, like alignment of lens with respect to focal plane after focus changes).

Figure 7 shows an example of reference star residuals as a function of magnitude. Data from an entire set of grating observations over five nights in 2013 December are shown for CCD A. Systematic position differences on the ± 10 mas level are seen. Plots for the other CCDs look almost identical. Remaining systematic errors in UCAC4 alone can explain these differences (Zacharias et al. 2013) and were expected to show up here owing to the poor charge transfer efficiency of the UCAC CCD. No "corrections" to URAT1 as a function of magnitude (over the nonsaturated regime) were applied here in order to not propagate such UCAC4 errors into URAT1.

Figure 8 shows the residuals of the same data set as a function of color. Most systematic differences are within ± 5 mas. The same types of plots of other data sets look similar. No corrections for differential color refractions (DCRs) were applied. From theoretical estimates the effect of DCR on URAT1 position data is found to be below our systematic error floor, which is confirmed by residual plots as a function of color. Figures 7 and 8 were generated after correcting for other systematic errors, as explained next.

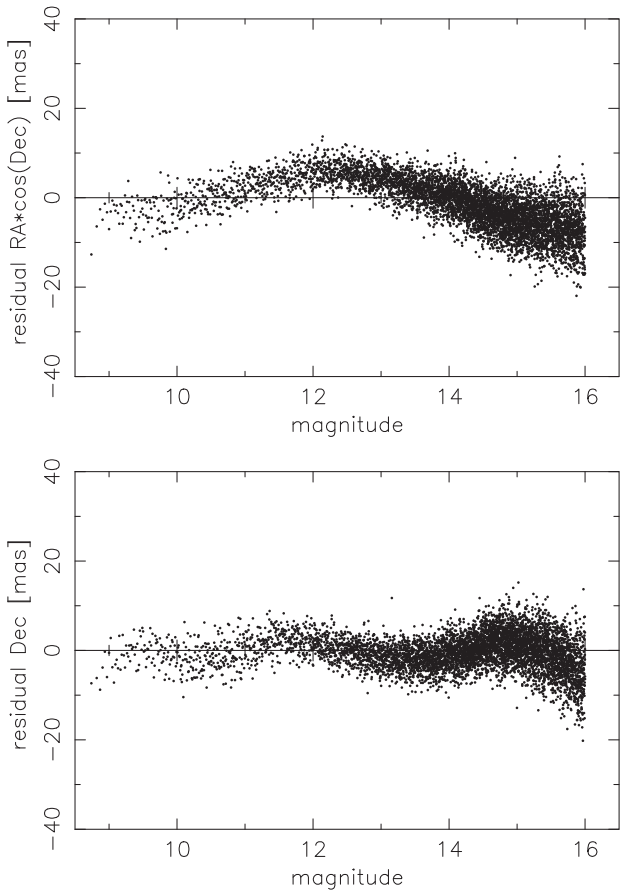

Figure 7. Example of residuals (URAT1–UCAC4) for all grating observations in set 13 (Julian date nights 6640 to 6644) of CCD A. Position differences (R.A. top, decl. bottom) are shown as a function of UCAC4 magnitude. Each dot is the mean over 1000 observations.

4. SYSTEMATIC ERROR CALIBRATION

4.1. Pixel Phase Error

Small systematic position errors as a function of the subpixel location of stellar image centers are seen in the astrometric solution residuals. As expected, these follow a sine curve as a function of pixel phase. The amplitude (A) of the sine curve is related to w, the FWHM of the image profile, by an exponential function:

$$A = ae^{-bw}.$$

The parameters a and b were determined from a linear least-squares fit to sample data, separately for each CCD and coordinate. For the smallest observed image profile width in URAT data, about 1.8 pixel FWHM, the maximal amplitude is about 20 mas. For typical data the amplitude is about 10 mas and quickly drops off to insignificant levels at FWHM $\geqslant$ 2.5 pixel.

Individual position corrections to URAT1 observations are then applied for each image and coordinate based on the sine function of pixel phase value and amplitude as derived for a given exposure's mean FWHM (from quality control data). Resulting residuals showed a small remaining effect, which

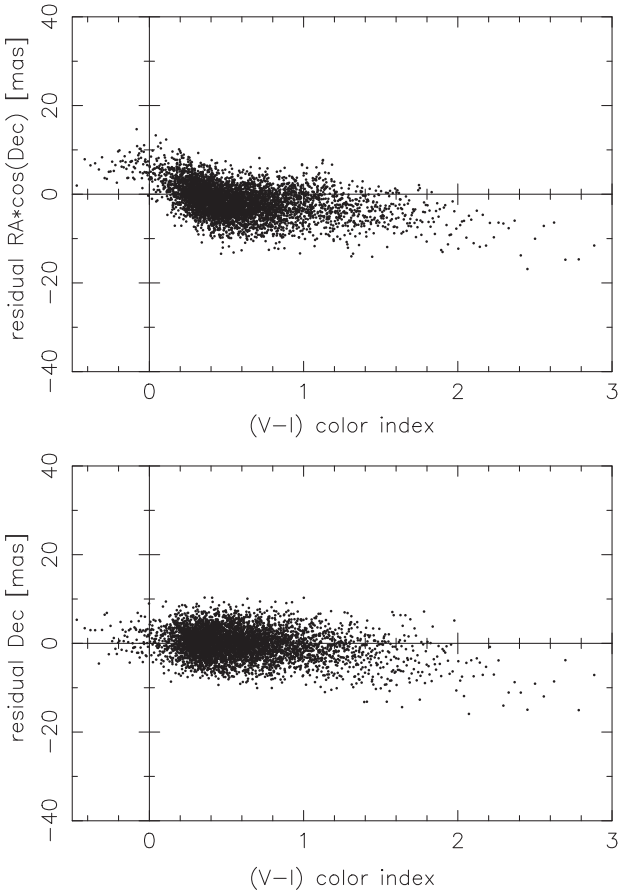

Figure 8. Same as previous figure, but for residuals as a function of *V–I* color index (from APASS data).

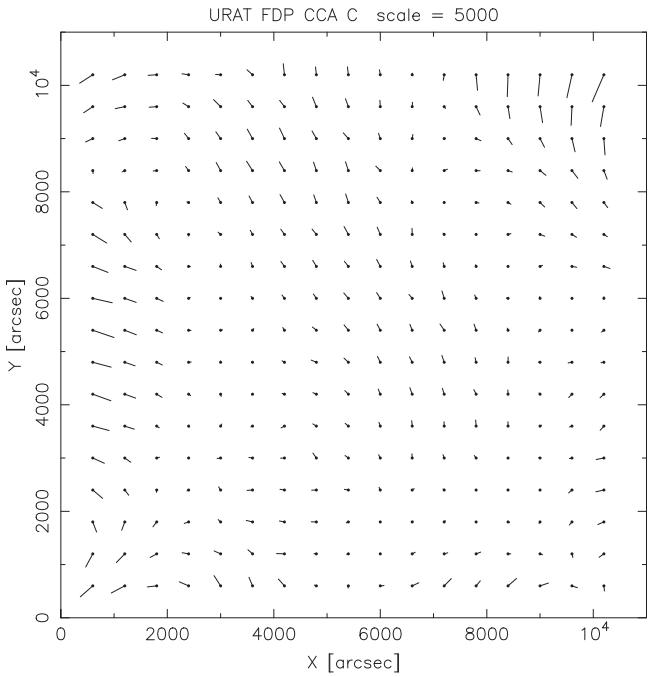

Figure 9. Mean field distortion pattern of CCD C as derived from residuals of a single night. The longest vector is about 80 mas.

Table 2
rms Systematic Position Offsets (millipixel) as a Function of Location in the Focal Plane (Field Distortion Pattern)

Coordinate	CCD A (mpx)	CCD B (mpx)	CCD C (mpx)	CCD D (mpx)
x	22	24	20	15
y	22	26	22	22

was corrected by updating the parameters for the pixel phase errors.

4.2. Field Distortion Pattern

Residuals of astrometric solutions using UCAC4 reference stars were stacked up as a function of *x*, *y* coordinate in the focal plane, separately for each CCD. Figure 9 shows an example of such a field distortion pattern (FDP) for CCD C based on residuals of 140 exposures of acceptable quality of a night in 2014 March. The position difference vectors were scaled by a factor of 5000. The FDPs of the four CCDs look different as a result of the combination of optical distortion (lens and dewar window) and individual tilt with respect to the ideal focal plane. However, the level of systematic errors is very similar for all four CCDs (Table 2).

Sample FDPs of data of the same night but split by magnitude, or color of stars, or by exposure time were identical within the random noise level of about 3–5 mas rms. Comparing data from different nights, or split by declination or early part versus later part of a night, displayed typical rms differences of about 5–10 mas with somewhat correlated vectors over the field of view. This result is not fully understood, but changing temperature gradients across the CCDs are suspected to play a role.

The FDPs of several nights were averaged to a mean FDP, which was applied to the *x*, *y* data. After application of the mean FDP, the residual FDP pattern was much smaller but seemed to still show some systematics. The process was iterated once to arrive at a single final FDP (per CCD), which was used for calibrating all URAT1 data.

4.3. General Magnitude Equations

Flip observations (Section 2.7) provide pairs of observations of the same area in the sky and the same CCD with *x, y* data in two orientations rotated by 180° between the data sets. Mapping between two such exposures was performed using a full second-order polynomial model (12 parameters) with over 1000 stars in a weighted least-squares adjustment. Residuals were then binned and plotted as a function of magnitude.

Figure 10 shows an example for CCD B and exposure pair 7999 versus 8015 (60 s). Larger-than-average scatter is seen at the very bright end (owing to few stars) and the faint end (owing to large *x*, *y* center errors). Note that traditional saturation is at about 6.5 mag on this scale. For stars brighter than that, the CAB feature allows for useful astrometric data.

If there were a pure magnitude equation (systematic position shift as a function of magnitude) caused by the instrument (lens plus camera and readout), those systematic errors would show up with doubled amplitude in these flip observations. A coma-like magnitude equation (systematic position shift as a function of the product of magnitude and *x, y* coordinate) would show up in the same way. For UCAC data, for example, the coma-like systematic errors are on the order of ±100 millipixels (mpx) over 6 mag caused by a poor charge transfer efficiency

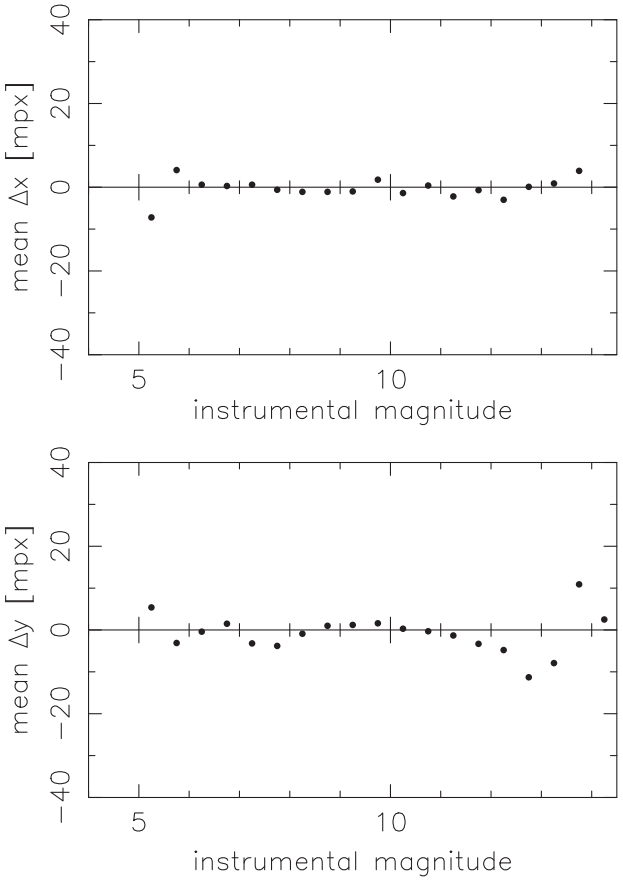

Figure 10. Position differences of a flip observation (pair of exposures, regular and 180° rotated with respect to sky) as a function of magnitude.

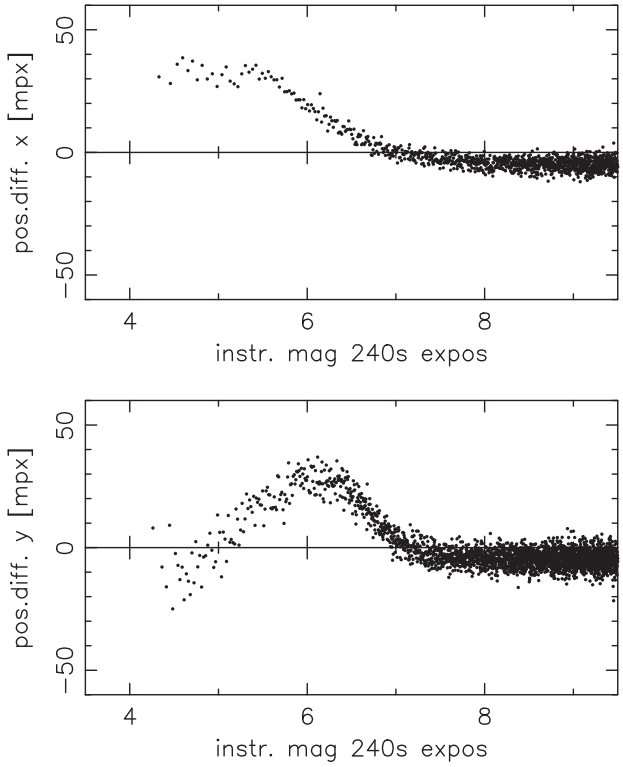

Figure 11. Position differences (x top, y bottom) between data from long (240 s) and short (60 s) regular survey exposures of the same fields. Results for a single night (JD 6828) are shown for CCD A. Each dot represents the mean over 250 stars. Saturation of the long and short exposure begins at magnitude 6.8 and 5.3, respectively, on this scale. Systematic position offsets within this range can be attributed to errors caused by saturation of the long exposure only.

of that CCD. With URAT1 data we see here nothing of significance, with an upper limit of about 10 mpx/2 = 5 mpx.

There is a degeneracy between a pure magnitude equation and a coma-like term as seen in these flip observations. If they are of exactly the same amplitude with opposite sign, they would cancel out and show a flat result like seen in Figure 9; however, that is very unlikely.

Plots for the other CCDs and other pairs of flip observations look very similar. There are no indications of a significant magnitude equation or coma-like term in URAT1 x, y data.

4.4. Grating Images

Differences between x, y positions of central images and first-order images of grating observations were calculated. Data from the same exposure were analyzed, which give only a small magnitude range with both zeroth- and first-order images having sufficient signal-to-noise ratio as well as not being saturated. Similarly, x, y transformations were performed between the zeroth-order data of 30 s exposures and 240 s exposures of first-order data to extend the range of overlapping magnitudes. In all investigations no systematic difference between the positions of zeroth- and first-order images was found.

4.5. Astrometric Calibration near Saturation

Although the CAB feature of our CCDs allows us to acquire positions of stars from successful x, y center fits up to about 2.5 mag brighter than saturation, those data are subject to systematic errors as compared to unsaturated data. Regular survey observing provides a short (60 s) and a long (240 s) exposure of each observed field. Thus, the long exposure saturates at about 1.5 mag earlier than the short exposure.

Using only stars of instrumental magnitude 12 or brighter, the x, y data of a long exposure are matched with the data of the short exposure using a linear transformation model. The residuals as a function of magnitude, separately for each CCD and coordinate, reveal the desired systematic position offset of saturated data with respect to unsaturated data. An example is given in Figure 11 for a single night and CCD A. Data for other CCDs look similar. Here the instrumental saturation magnitude is near 6.8. In the range of 6.8–5.3 mag the short exposure is still unsaturated and is assumed to be "error free." The position difference seen in that range thus shows the systematic error of the long exposure beyond the traditional saturation. For instrumental magnitudes brighter than 5.3 mag the short exposure also becomes saturated and begins to show the same relative offset (with respect to error free) as the long exposure. Assuming that the (observed long exposure−true) position difference continues on a linear function with magnitude for stars brighter than (saturation mag—1.5 mag), we would expect to see a constant position difference in these plots for stars brighter than about 5.3 mag. That is what we see for the x-coordinate in our example.

For the y-coordinate in Figure 11 we see a drop in the observed position differences for stars brighter than about instrumental magnitude 5.3, indicating an actual deviation from the simple linear position correction model. Empirical

Table 3
Characteristics of the URAT1 Catalog

Data Items		Value
Total numb. URAT1 stars	=	228276482
Number stars with 1 obs	=	10309229
Number stars with 2 obs	=	8875122
Average numb. obs/star	=	24.3
Number valid 2MASS data	=	188656145 82.64%
No 2MASS match stars	=	39620337 of
Stars >=3 obs., no 2MASS	=	39079551 URAT1
Number valid APASS data	=	37010348 16.21%
APASS stars valid B mag	=	29313850 of
APASS stars valid V mag	=	30057593 URAT1
APASS stars valid g mag	=	32340624 stars
APASS stars valid r mag	=	32474206
APASS stars valid i mag	=	28052917

corrections were derived based on two linear stretches in the overexposed magnitude regime, with corresponding free parameters for the magnitudes at which each linear stretch begins and ends (i.e., 3 mag and two slope parameters total).

Data from different nights were analyzed, showing a break in the pattern, some of which corresponds to changes in the camera electronics (swap or replacement of boards that control the readout of the main camera CCDs). Some data show position offsets exceeding 100 mas at about 2 mag brighter than traditional saturation; others show total errors of only about 10 mas. A total of six groups as a function of epoch could be identified. Separate systematic position error corrections for the overexposure regime were derived for the data in each of the groups and for each CCD and coordinate. The corrections were then checked against the observed residuals of astrometric solutions using UCAC4 reference stars. Remaining systematic errors are expected to be $\leqslant$10 mas up to about 1.5 mag brighter than traditional saturation and somewhat larger for even brighter stars.

5. THE CATALOG

Some basic numbers of the URAT1 catalog are given in Table 3. The URAT1 data are provided by binary zone files each covering 0°.2 along declination. Each entry has 80 bytes of integer data, which is explained in Table 4. Sample files in ASCII, a detailed "readme" file, index files, and basic access code are provided with the public release. URAT1 is not distributed by USNO but instead is kindly served by CDS, Strasbourg, through Vizier as catalog I/329. The distribution of URAT1 stars by magnitude is shown in Figure 12.

5.1. Mean Positions

Weighted mean positions were obtained separately for each of the 38 data sets (see above) from the astrometric solutions after having applied systematic error corrections for pixel phase error, field distortions, and stars in the CAB regime. These positions were then combined to a weighted overall mean position given in the URAT1 catalog. Thus, URAT1 is an observational catalog providing positions on the International Celestial Reference Frame (ICRF) via UCAC4 reference stars, which are believed to be on the *Hipparcos* system. The mean epoch of stars in URAT1 is slightly different for each star within the range of 2012.3–2014.7. Most stars have a mean epoch closer to the center of that range, but some objects were observed only early or late within this range (sky coverage, limiting magnitude).

To make it into the catalog, a star needs to have at least three observations or a match with the 2MASS point-source catalog within 3 arcsec. The average number of observations per star is 24. The distribution of URAT1 position errors (from scatter of individual observations) is shown in Figure 13.

5.2. Proper Motions

Preliminary proper motions were calculated exclusively from combining the observed, mean URAT1 positions with 2MASS positions at about 15 years earlier. Typical proper motion errors are about 5–7 mas yr^{-1} (see Figure 14). The proper motion errors given in the URAT1 catalog are formal errors based on the individual epoch difference and positional errors of the two catalogs involved, assuming a constant 80 mas error for 2MASS data independent of brightness. Note that stars with few observations (like 1 or 2) and large proper motions in URAT1 need to be taken with caution, particularly in crowded areas, because of possible accidental (wrong) matches with 2MASS entries.

5.3. Added Data

URAT1 observational data are supplemented by 2MASS *J, H,* and K_s magnitudes and some 2MASS flags for about 83% of stars in common. APASS provided *B, V, g, r, i* magnitudes for about 16% of the URAT1 stars. The APASS photometry is taken from DR8 plus single observations not yet published elsewhere.

5.4. Contamination and Completeness

Possible reasons for false entries in URAT1 include issues with close doubles/blended images, minor planets, CCD defects, artifacts near bright stars, and contamination from the grating image assignment process. An upper limit of the number of false objects in URAT1 is estimated by the list of 1.1 million objects not found in GSC 2.4 (see below), which is less than 0.5% of the URAT1 catalog entries.

URAT1 is not complete, even in the areas covered by observations. Blended images, close double stars, and any "problem" case during the reductions were just dropped. The goal here is to provide the user with an accurate, dense reference star catalog at current epochs.

6. EXTERNAL COMPARISONS

The URAT1 catalog as of 2014 November was extensively validated in-house and by selected external reviewers. Results for positions and proper motions are summarized in Table 5.

6.1. Primary Systems

At the bright end URAT1 was compared directly to the *Hipparcos* Catalog (van Leeuwen 2007). No significant mean position differences (within about 5 mas) were found, confirming the URAT1 catalog to be on the *Hipparcos*/ICRF system. Observed URAT1 positions of over 66,000 stars in common with the *Hipparcos* Catalog were compared at the URAT1 mean observational epoch using the *Hipparcos* Catalog positions and proper motions. For more details see Zacharias (2015) and Frouard et al. (2015).

Table 4
Description of Data Items Contained in the URAT1 Catalog

Col	Item	Type	Unit	Description
1	ra	I*4	mas	Mean RA on ICRF at URAT1 obs.epoch
2	spd	I*4	mas	Mean South Pole Distance
3	sigs	I*2	mas	Position error per coord.(scatter)
4	sigm	I*2	mas	Position error per coord.(model)
5	nst	I*1	-	Tot. number of sets star is in
6	nsu	I*1	-	n. of sets used for mean position
7	epoc	I*2	myr	Mean URAT1 obs. epoch − 2000.0
8	mmag	I*2	mmag	Mean URAT1 model fit magnitude
9	sigp	I*2	mmag	URAT1 photometry error
10	nsm	I*1	-	n. of sets used for URAT1 magnitude
11	ref	I*1	-	Largest reference star flag
12	nit	I*2	-	Total number images (observations)
13	niu	I*2	-	n. of images used for mean position
14	ngt	I*1	-	Total n. of first-order grating obs.
15	ngu	I*1	-	n. of first-order grating obs. used
16	pmr	I*2	0.1mas/yr	Proper motion RA*cosDec
17	pmd	I*2	0.1mas/yr	Proper motion Dec
18	pme	I*2	0.1mas/yr	Proper motion error per coord.
19	mf2	I*1	-	Match flag URAT1 with 2MASS
20	mfa	I*1	-	Match flag URAT1 with APASS
21	id2	I*4	-	2MASS star identification number
22	jmag	I*2	mmag	2MASS J mag
23	hmag	I*2	mmag	2MASS H mag
24	kmag	I*2	mmag	2MASS K mag
25	ejmag	I*2	mmag	Error 2MASS J mag
26	ehmag	I*2	mmag	Error 2MASS H mag
27	ekmag	I*2	mmag	Error 2MASS K mag
28	iccj	I*1	-	CC flag 2MASS J
29	icch	I*1	-	CC flag 2MASS H
30	icck	I*1	-	CC flag 2MASS K
31	phqj	I*1	-	Photometry quality flag 2MASS J
32	phqh	I*1	-	Photometry quality flag 2MASS H
33	phqk	I*1	-	Photometry quality flag 2MASS K
34	abm	I*2	mmag	APASS B mag
35	avm	I*2	mmag	APASS V mag
36	agm	I*2	mmag	APASS g mag
37	arm	I*2	mmag	APASS r mag
38	aim	I*2	mmag	APASS i mag
39	ebm	I*2	mmag	Error APASS B mag
40	evm	I*2	mmag	Error APASS V mag
41	egm	I*2	mmag	Error APASS g mag
42	erm	I*2	mmag	Error APASS r mag
43	eim	I*2	mmag	Error APASS i mag
44	ann	I*1	-	APASS numb. of nights
45	ano	I*1	-	APASS numb. of observ.

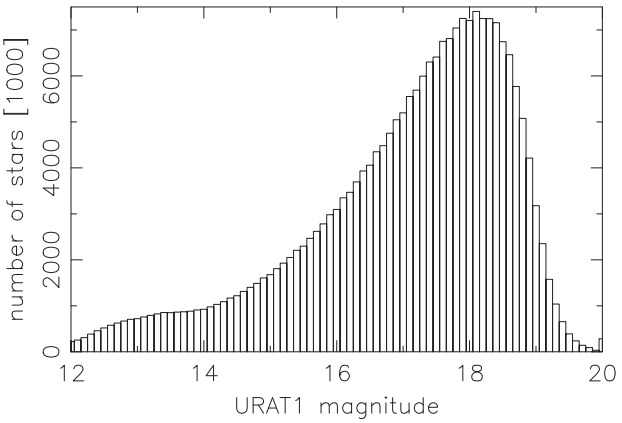

Figure 12. Distribution of URAT1 stars by magnitude.

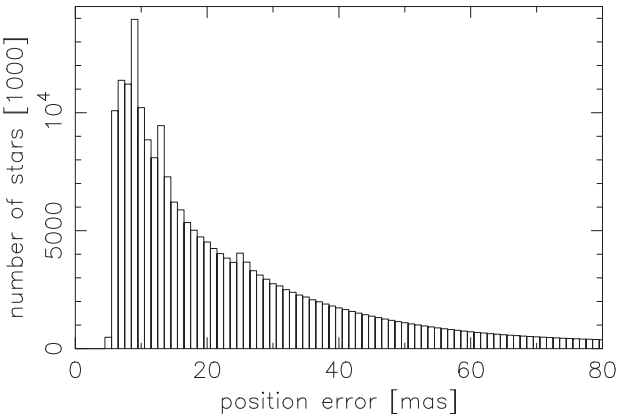

Figure 13. Distribution of URAT1 position errors.

At the faint end URAT1 provided observations of 958 ICRF2 (Fey et al. 2009) counterparts. Excluding outliers, mean URAT1 positions of the remaining 849 sources are consistent with the ICRF within about 10 mas (see Figure 15). This is the single largest systematic error seen with URAT1 so far, and a more detailed investigation including more extragalactic radio sources is under way. However, these data indicate an upper limit of a possible magnitude-dependent systematic error in URAT1 over its large range of over 12 mag (*Hipparcos* stars to faint-end ICRF sources) of about 10 mas for decl. and less than that for R.A.

URAT1 proper motions of the ICRF sources are around zero, as expected (Figure 16). Similarly, over 14,000 extragalactic sources of the second Large Quasar Astrometric Catalog (LQAC2; Souchay et al. 2012) are found in URAT1. Their observed mean proper motions as a function of declination zone and magnitude are typically within ± 0.5 mas yr^{-1} and up to about 2 mas yr^{-1} for some samples. A position comparison of these sources is not meaningful because of the relative low quality of LQAC2 positions as compared to URAT1.

6.2. Deep Catalogs

For the comparison with the PPMXL catalog, two zones around R.A. = 90° (z1) and 300° (z2) going over all declinations and covering the 10–19 mag range were selected. Comparing PPMXL with ICRF2, large systematic differences

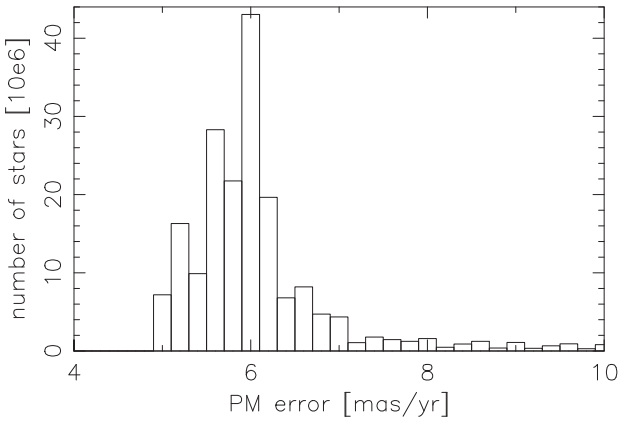

Figure 14. Distribution of URAT1 proper motion errors.

Table 5
Summary of External Comparisons of URAT1 Catalog Data

Positions:				
Catalog	dRAcos(D) (mas)		dDec (mas)	
	Bright	Faint	Bright	Faint
ICRF2	+6 (12)	−4 (19)	+3..−2..	+12..+7
Hip.2 0	(8)	...	+5 (8)	...
PPMXLz1	0 ..+5..	0 ..+20	0 ..−10..	−10.. −20
PPMXLz2	+5.. +10..	+5..+15	+10.. −10..	−25.. −10
SDSS	+9 (14)	−8 (19)	−6 (14)	+8 (19)
PM2000	+2 (9)	0 (15)	+10 (10)	+12 (15)

Proper Motions:				
Catalog	dRAcos(D) (mas yr^{-1})		dDec (mas yr^{-1})	
	Bright	Faint	Bright	Faint
ICRF2	+2.0 .. −2.0 .. 0.0		−0.5 (12)	+0.5 (18)
LQAC2	+2.2 (12)	−0.2 (19)	−0.5 (14)	0.0 (19)
LSPMa	0.0 (8)	−0.5 (18)	+1.0 (8)	+4.0 (18)
LSPMr	−2.0 (8)	−2.0 (18)	−7.0 (8)	−3.0 (18)
PPMXLz1	0.0..+0.5..−1.0		−0.8.. 0.0..+1.0	
PPMXLz2	+0.5..+1.0..−0.5		0.0..−0.8..+1.0	
SDSS	+1.0 (14)	−0.1 (19)	−1.7 (14)	−0.2 (19)
PM2000	+1.0 (9)	0.0 (16)	0.0 (9)	+1.2 (15)

Note. Numbers in parentheses indicate the URAT1 magnitude.

up to about 40 mas are seen, suggesting that some of the observed URAT1–PPMXL differences are caused by errors in the PPMXL.

An extensive comparison to the Sloan Digital Sky Survey (SDSS) data (Munn et al. 2004) was performed. Positions are compared at the URAT1 observational epoch by using USNO-B proper motions to update SDSS positions. Overall, the systematic differences in proper motions are about 0.4 and 0.9 mas yr^{-1} for R.A. and decl., respectively, with variations as a function of field on the sky with a standard deviation of 1.8 mas yr^{-1}. The differences in positions are correlated with

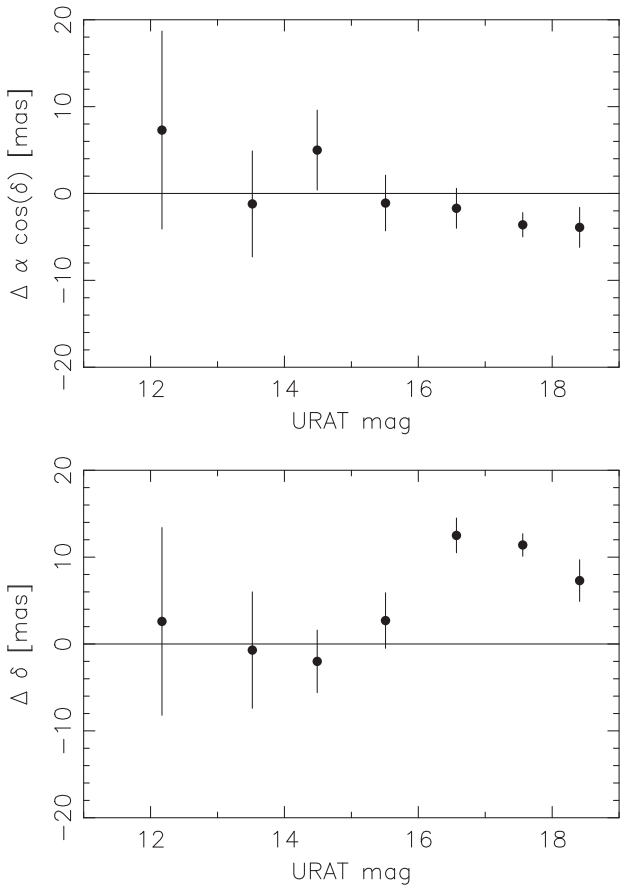

Figure 15. Weighted mean position differences URAT1–ICRF2 of optical counterparts directly observed with the astrograph.

the proper motion differences, and a small magnitude equation is seen in each coordinate (about ±8 mas between magnitude 14 and 19).

A match of the URAT1 stars with GSC 2.4 was performed (R. Smart 2014, private communication). A total of 1.1 million URAT1 entries are not found in the GSC data, which is believed to be very "clean" and complete. A spot check of about 30 of those objects (random selection) versus the real sky reveals a mix of different cases. Some objects are clearly seen on the digital sky images, some are in crowded fields, and others point to very faint objects, no object at all, or close to an object, indicating a possible large proper motion. Thus, not all but an unknown fraction of these 1.1 million objects could be artifacts, or images of moving objects in URAT1. This result sets a limit of the contamination level in URAT1. Likely over 99.5% of URAT1 objects are real, stellar, or extragalactic sources.

6.3. PM2000

A detailed comparison of URAT1 data with the PM2000 catalog (Ducourant et al. 2006) was performed (C. Ducourant & R. Teixeira 2015, private communication). The PM2000 catalog covers the Bordeaux Zone ($+11° \leqslant \delta \leqslant +18°$) of the Astrographic Catalog (AC) project from around 1900. The AC plates were reduced with *Hipparcos* and combined with epoch near 2000 transit circle CCD data to arrive at positions and proper motions for stars in the about 7–16 mag range on the ICRF using a global adjustment. Thus, these data are completely independent of URAT1 and UCAC4. URAT1

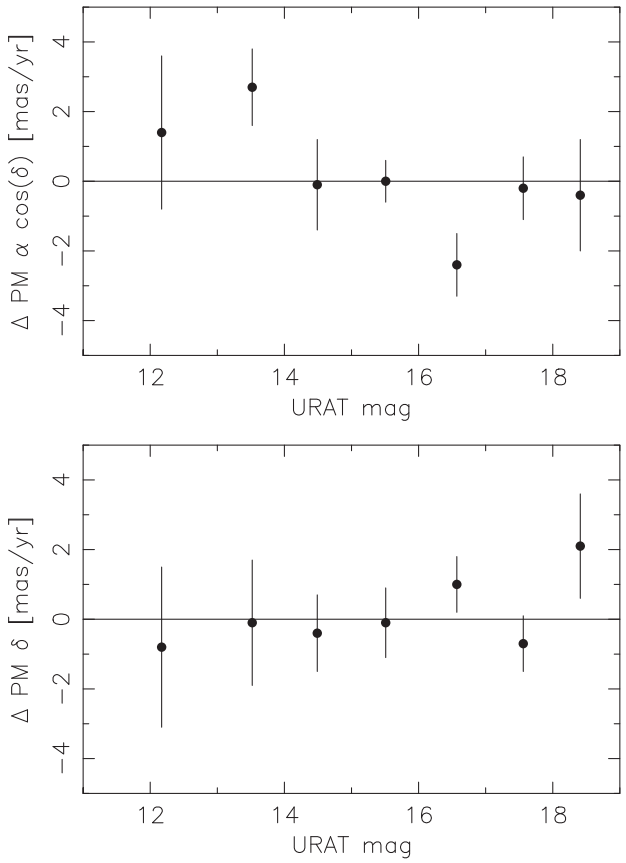

Figure 16. Mean URAT1 proper motions of the same ICRF2 counterparts as used for the previous figure.

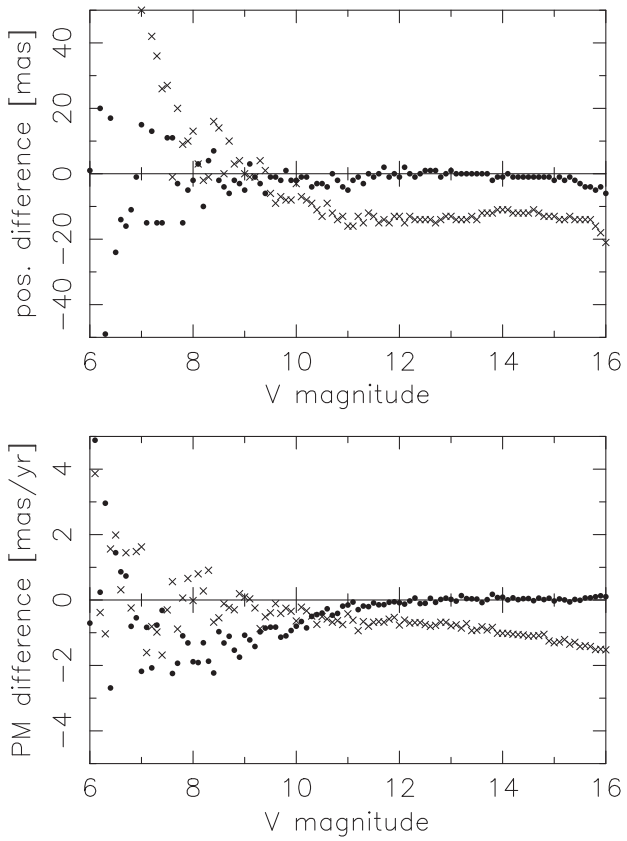

Figure 17. Mean PM2000–URAT1 position (top) and proper motion (bottom) differences as a function of *V* magnitude. Differences for R.A. are shown with filled circles, while the crosses represent the differences for the decl. coordinate.

agrees with PM2000 extremely well for R.A., with systematic position differences $\leqslant$5 mas over the 8–16 mag range (Figure 17) and as a function of R.A., with no magnitude equation. An almost constant position offset of about 10–15 mas is seen for decl., again with no magnitude equation. Large position differences of up to 50 mas in decl. are seen between PM2000 and URAT1 at the bright limit magnitude of PM2000 ($V = 7$). This is not seen when comparing URAT1 with *Hipparcos* directly.

The systematic proper motion differences between URAT1 and PM2000 are between 0 and 1.2 mas yr^{-1}. A noticeable increase in the rms proper motion differences is seen in the galactic plane, which can be explained by confusion of URAT1 to 2MASS matches and thus contaminating the sample with some false proper motions.

6.4. Other Comparisons

Over 57,000 stars of the Lepine and Shara Proper Motion (LSPM) catalog (Lépine & Shara 2005) are found in URAT1. Owing to the respective cutoffs of the catalogs, only stars with proper motions in the approximately 150–250 mas yr^{-1} range are seen. Both the LSPM relative and absolute proper motions were compared with URAT1. There is good agreement for R. A. but not for decl.

Vector point diagrams were derived from URAT1 data (R. Teixeira 2015, private communication) using 48 near-equal-area regions on the sphere. Except for the overdensity of proper motions around 200 mas yr^{-1} (again likely a contamination issue in crowded fields), the main result is that statistical behavior of URAT1 data is consistent with predictions of the Galaxy model (Besancon model). No abnormalities are seen in the spacial distribution of URAT1 proper motions.

Minor planet occultation predictions were analyzed (D. Harald 2014, private communication). Compared with previously used UCAC4 data, a noticeable improvement for the sample of 90 events observed in the past is seen when using URAT1 data. This check on many random fields indicates good astrometric performance of URAT1 data for applications that are sensitive on the 10 mas level of accuracy.

7. DISCUSSION AND CONCLUSIONS

The distribution of URAT1 proper motions on the sky shows the effects of solar motion and galactic rotation and thus gives some confidence in the overall accuracy of URAT1 astrometry (no significant spacial biases). Systematic differences of proper motions between URAT1 and several other external data are on the 1–2 mas yr^{-1} level. At this point it is not clear which data set has the smallest systematic errors.

The systematic position error floor of URAT1 data is likely around 10 mas. URAT1 data match the current celestial reference frame at the bright end (*Hipparcos* Catalog) and the faint end (ICRF counterparts) very well, which suggests insignificantly small magnitude equations in URAT1 data. Local, spacial systematic errors of URAT1 positions and proper motions have not been investigated in detail. However, such errors are not to be expected owing to the "averaging" URAT observing method (same star imaged on different CCDs and

different parts of a CCD) and the homogeneous astrometry of 2MASS.

URAT1 has a very low level of contamination by false entries (few tenths of a percent at most), as seen from comparisons with the GSC and other data. Possibly some minor planets have made it into the catalog. Other false objects will include artifacts near bright stars or detections associated with blended images. Some proper motions in URAT1 will be wrong owing to mismatches with 2MASS, particularly in dense fields. URAT1 is not intended to be complete but should be complete to over 90% in the sky area covered and 3–18 mag range owing to the observing and reduction methods used.

URAT1 can serve as accurate reference star catalog before *Gaia* data become available. The position accuracy of URAT1 is about four times higher than for UCAC4 data at its faint end, and the sky density of URAT1 is about 4 times larger than that of UCAC4, similar to the sky density of 2MASS.

The USNO management is thanked for supporting this project: K. J. Johnston, B. Luzum (the former and current scientific directors of USNO), R. Gaume, B. Dorland (the former and current head of the astrometry department), and P. Shankland (the director of NOFS). Semiconductor Technology Associates (headed by R. Bredthauer) provided continued support for the URAT camera and dewar long after delivery. The American Association of Variable Star Observers (AAVSO) is thanked for providing unpublished APASS data for our project. 2MASS was used for near-IR photometry and as the first epoch of URAT1 proper motions. Bill Gray (Project Pluto) is thanked for making available a C-code version of our URAT1 access software: www.projectpluto.com/urat.htm. Aladin and Vizier were invaluable tools provided through CDS, Strasbourg. CDS Strasbourg is also thanked for hosting the URAT1 catalog. DS9 by the Smithsonian Astrophysical Observatory was used as a display tool for FITS pixel data files. NOAO is thanked for IRAF, which was used for image analysis while troubleshooting and performing spot checks. Pgplot by California Institute of Technology was used to produce plots.

REFERENCES

Ducourant, C., Le Campion, J. F., Rapaport, M., et al. 2006, A&A, 448, 1235
Fey, A., Gordon, D., & Jacobs, C. S. (ed.) 2009, IERS Tech. Note 35 (Frankfurt: Harri Deutsch)
Frouard, J., Dorland, B., & Makarov, V. V. 2015, AJ, submitted
Laux, U., & Zacharias, N. 2005, in Proc. ASP Conf. Ser. 338, Astrometry in the Age of the Next Generation of Large Telescopes, ed. K. Seidelmann & A. K. B. Monet (San Francisco, CA: ASP), 184
Lépine, S., & Shara, M. M. 2005, AJ, 129, 1483
Munn, J., Monet, D. G., Levine, S. E., et al. 2004, AJ, 127, 3034
Skrutskie, M. F., Cutri, R. M., Stiening, R., et al. 2006, AJ, 131, 1163
Souchay, J., Andrei, A. H., Barache, C., et al. 2012, A&A, 537, 99
van Leeuwen, F. 2007, Hipparcos, the New Reduction of the Raw Data (Astrophysics and Space Science Library, Vol. 350; Berlin: Springer)
Vukobratovich, D., Valente, T., Shannon, R. R., Hooker, R., & Sumner, R. E. 1992, Proc. SPIE, 1752, 245
Zacharias, N. 2002, Proc. SPIE, 4836, 279
Zacharias, N. 2004, AN, 325, 631
Zacharias, N. 2015, in Proc. ADeLA 2014 meeting, in press (arXiv:1506.05853)
Zacharias, N., Finch, C. T., Girard, T. M., et al. 2013, AJ, 145, 44
Zacharias, N., Laux, U., Rakich, A., & Epps, H. 2006, Proc. SPIE, 6267, 227